



CHORUS

This is the accepted manuscript made available via CHORUS. The article has been published as:

Thermotropic liquid crystal (5CB) on two-dimensional materials

Paul A. Brown, Sean A. Fischer, Jakub Kołacz, Christopher Spillmann, and Daniel Gunlycke
Phys. Rev. E **100**, 062701 — Published 12 December 2019

DOI: [10.1103/PhysRevE.100.062701](https://doi.org/10.1103/PhysRevE.100.062701)

Thermotropic liquid crystal (5CB) on two-dimensional materials

Paul A. Brown

ASEE Post-Doctoral Fellow at the U.S. Naval Research Laboratory, Washington, DC 20375

Sean A. Fischer, Jakub Kołacz, Christopher Spillmann, and Daniel Gunlycke*

U.S. Naval Research Laboratory, Washington, DC 20375, USA

We present ground-state electronic properties of the liquid crystal 4-cyano-4'-pentylbiphenyl (5CB) on the two-dimensional materials monolayer graphene, hexagonal boron nitride, and phosphorene. Our density functional theory results show that the physisorption is robust on all surfaces with the strongest binding of 5CB on phosphorene. All surfaces exhibit flexural distortion, especially monolayer graphene and hexagonal boron nitride. While we find type-I alignment for all three substrates, meaning the Fermi level of the system is in the HOMO-LUMO gap of 5CB, the band structures are qualitatively different. Unlike for graphene and phosphorene, the HOMO-LUMO of 5CB appear as localized states within the band gap of boron nitride. In addition, we find that the valence band for boron nitride is sensitively to the orientation of 5CB relative to the surface. The qualitatively different band structures demonstrate the importance of substrate selection for tailoring the electronic and optoelectronic properties of nematic liquid crystals on two-dimensional materials.

I. INTRODUCTION

Liquid crystals have a long established history in display technologies owing to their responsiveness to external electric fields [1]. Of late, liquid crystals have extended beyond LCDs to nascent technologies such as sensors [2, 3], optoelectronic devices [1, 4–7], lenses [8], diffraction gratings [3, 9, 10], colloidal templating [11], and metamaterials [1, 12]. These new advances reflect the versatility of liquid crystal phases and signal opportunities for combining liquid crystals with emerging materials.

Nanosheets of two-dimensional (2D) materials have flourished into a new frontier for the scientific community [13, 14], and there are efforts to use these nanosheets with both existing or emerging technologies [15–18]. These efforts include experiments combining 2D materials and liquid crystals [19–31]. Basu *et al.* [23] introduced monolayer graphene into a conventional liquid crystal cell to operate as an alignment layer and electrode, thereby reducing the size of the electrode and enhancing the director field response. Subsequently, Naqvi *et al.* [27] developed a technique to observe oxidative degradation of phosphorene, as is common for group-V 2D materials when exposed to air. These experimental works have mostly focused on demonstrating the usefulness of combining liquid crystals and 2D materials, without yet addressing the fundamentals of why there is a synergy between them. Additionally, the computational studies to date have mainly addressed the orientation of adsorption geometries. To advance progress and really leverage the properties of each material, a fundamental understanding of the electronic structure of a mesogen interacting with a 2D material is needed.

Herein, we explore the electronic ground-state properties of a well-known thermotropic liquid crystal on three

separate 2D materials. Specifically, we select 4-cyano-4'-pentylbiphenyl (5CB) as a representative liquid crystal and monolayer graphene (G), hexagonal boron nitride (BN), and phosphorene (BP), as our three substrates. These are some of the most studied 2D materials in general and in particular have already been explored for use with liquid crystals [20, 23, 27]. For each substrate, we have identified four binding structures. The armchair (AC), intermediate (INT), and zig-zag (ZZ) structures, named after the orientations of the mesogens relative to the substrates, have all been found to be geometrically stable [32]. For comparison, we have also included a fourth eclipsed (ECL) structure oriented along an armchair direction, but with the phenyl rings in register with the underlying substrates. The electronic properties of the chosen structures and substrates have been determined using periodic density functional theory (DFT). For all three substrates, we find a robust physisorption of 5CB parallel to the surfaces with the strongest binding on BP. Moreover, the binding in all cases is dominated by dispersive interactions inducing interfacial dipoles within the equilibrium structures, which we observe through fluctuations in the planar-averaged charge density. In addition, our calculations indicate that a 5CB mesogen binding causes an out-of-plane distortion (or flexion) of the substrate, although limited in the case of BP owing to its planar truss structure. There is also a significant difference between G and BN for the ECL structure, suggesting the presence of a significant electromechanical component.

These and other findings are presented in sections below, which are organized as follows. Section II presents the methods used in our calculations. Then, in Sec. III, we present and discuss the main results. From these results, we then draw some final conclusions in Sec. IV.

* daniel.gunlycke@nrl.navy.mil

II. METHOD

The calculations of 5CB/substrate were performed using first-principles DFT within the projector-augmented wave method in the Vienna ab initio simulation package (VASP-5.4.1) [33–36]. All 2D crystals were set to have an orthorhombic 8×6 supercell to accommodate 5CB within the cell. We have included a vacuum space of 34 \AA to mitigate periodic image effects. The exchange-correlation functional applied throughout this work is the Perdew-Burke-Ernzerhof (PBE) generalized gradient approximation [37, 38]. Furthermore, because semi-local functionals do not adequately capture long-range dispersive interactions, we include Grimme’s D3 van der Waals correction with Becke-Jonson damping [39, 40]. Each system was optimized with a cutoff energy of 600 eV for the plane-wave basis. The forces were optimized until the tolerance of 0.01 eV \AA^{-1} was reached. The k -space sampling is a Γ -centered grid for geometry optimization, and the k -points sampling is increased to a $12 \times 12 \times 1$ k -grid for projected density of states (DOS), and binding energy estimates with the tetrahedron method with Blöchl corrections [41]. The binding energy (E_B) was calculated using

$$E_B = E_{5\text{CB}/c} - (E_{5\text{CB}} + E_c), \quad (1)$$

where $E_{5\text{CB}/c}$ is the ground state energy of the composite 5CB/substrate cell, and $E_{5\text{CB}}$ and E_c are the ground state energies of the 5CB mesogen and the 2D substrate, respectively, isolated from each other within identical cells. [32]. From the ground state equilibrium geometries, we calculate the planar-averaged charge density from

$$\Delta\bar{\rho}_z = \frac{1}{\Omega_{xy}} \int [\rho_{5\text{CB}/c} - (\rho_{5\text{CB}} + \rho_c)] dx dy, \quad (2)$$

where Ω_{xy} is the area of the cell in the plane of the substrate, $\rho_{5\text{CB}/c}$ is the charge density for the composite system, $\rho_{5\text{CB}}$ is the charge density of the isolated 5CB, ρ_c is the charge density of the isolated substrate, and $dx dy$ is an infinitesimal Cartesian area element. Lastly, we applied Bader analysis to study the charge transfer between the mesogen and substrate [42, 43]. We include supplemental information containing all structures shown in Fig. 1, whereas the following results show the lowest energy configurations. The larger dataset containing the structures covered herein are found in the Supplemental Material [44].

III. RESULTS AND DISCUSSION

III.1. Graphene

We focus first on the adsorption of 5CB on G. Figure 1(a)–(d) shows top and side views of the geometry optimization of our four different 5CB/G structures.

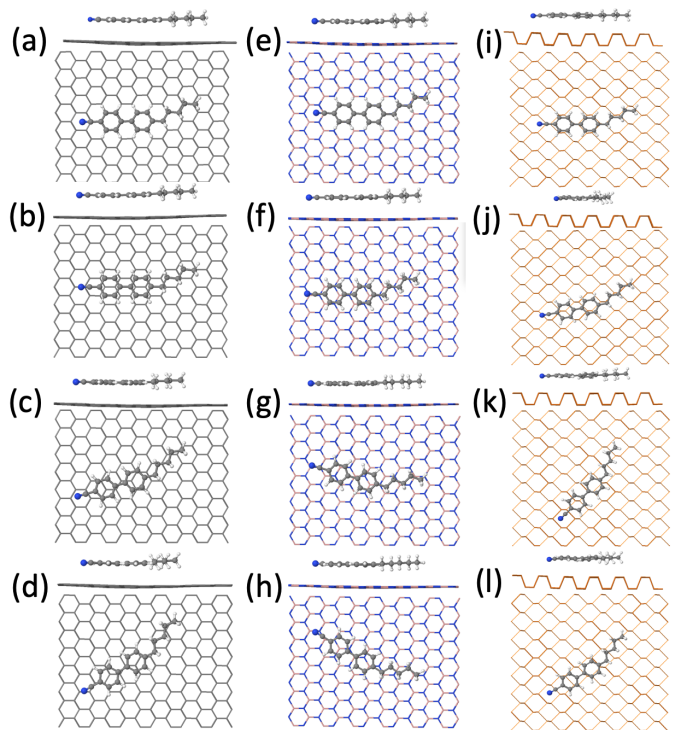


FIG. 1. Optimized geometry of 5CB on (a)–(d) G, (e)–(h) BN, and (i)–(l) BP. The structures are in top-to-bottom order ECL, AC, INT, and ZZ.

TABLE I. The nanosheet flexion along the z -axis degree-of-freedom (Δd), equilibrium mesogen-nanosheet distances (d_{vdW}), and biphenyl (Ph) dihedral angles (θ^{Ph}). The distances are taken from the cyano nitrogen to the nearest substrate element.

		Δd [\AA]	d_{vdW} [\AA]	θ^{Ph} [deg]	E_B [eV]
G	ECL	0.66	3.39	0.289	-1.264
	AC	0.26	3.36	1.010	-1.306
	INT	0.25	3.29	0.623	-1.327
	ZZ	0.27	3.31	0.241	-1.315
BN	ECL	0.22	3.38	-2.728	-1.182
	AC	0.17	3.26	-5.875	-1.242
	INT	0.20	3.28	-3.201	-1.229
BP	ZZ	0.17	3.38	-4.626	-1.213
	ECL	0.13	3.35	-19.34	-1.440
	AC	0.07	3.23	-16.61	-1.471
	INT	0.10	3.22	-16.78	-1.526
	ZZ	0.07	3.23	-19.16	-1.442

As can be seen in Table I, these structures have equilibrium distances d_{vdW} between the mesogen and substrate, herein defined as the distance between the nitrogen in 5CB and the nearest substrate site, ranging from 3.29 \AA to 3.39 \AA . These equilibrium distances are consistent for all three substrates and are in the typical range for physisorbed molecules. The biphenyl dihedral angles θ^{Ph} of 5CB on G, which range from 0.241° to 1.01° , are

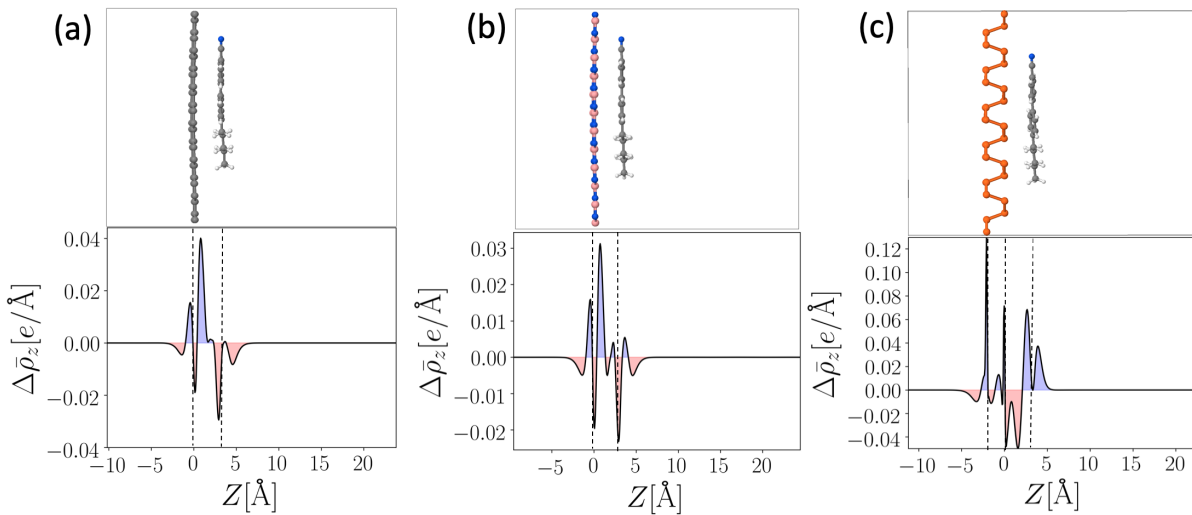


FIG. 2. Planar-averaged charge density differences for (a) INT-5CB/G, (b) AC-5CB/BN, and (c) INT-5CB/BP. Positive and negative regions of charge fluctuation are shown in blue and red respectively. Dotted lines trace the relative positions of 5CB and 2D material to aid the eye on the locations of each substance and van der Waals spacing.

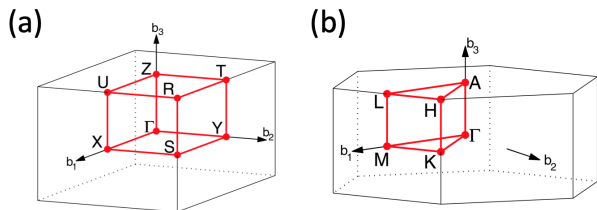


FIG. 3. Brillouin zones for tetragonal and hexagonal crystals. (a) Tetragonal Brillouin zone for the structures presented in the figures and (b) hexagonal Brillouin zone for G and BN comparison, see Fig. 5.[45]

nearly eclipsed at zero. Moreover, the eclipsed biphenyls are parallel to the graphene surface, which is to be expected, as this conformation maximizes the aggregate of the carbon-carbon interactions between the 5CB and graphene. For each structure, 5CB/G yields binding energies from -1.327 eV to -1.264 eV. These energies correspond approximately to -70 meV and -67 meV, respectively, per non-hydrogen atom [46], which are on the high end of the typical physisorption energies. The difference in binding energy of 5CB on the lowest energy configuration, INT, and the highest energy configuration, ECL, is $\Delta E_B^{(G)} = 62$ meV, which is approximately $2.4 k_B T$ at ambient conditions, for which $k_B T = 25.7$ meV. Because the ECL structure is stable, there must exist barriers exceeding $\Delta E_B^{(G)}$ between different 5CB positions on graphene. It is therefore reasonable to expect that the barriers between different orientations are large enough to prevent spontaneous mesogen reorientation under ambient conditions, even though the energy differences between the AC, INT, and ZZ structures on G observed in experiment are smaller than $k_B T$ [32]. We note that the small energy differences amongst the configurations preclude us from asserting that one configuration is really more stable than

another as different exchange-correlation approximations will possibly give different orderings [26]; however, what is consistent is that the observation of multiple orientations are expected to have substantial population under ambient conditions due to the near degeneracy of the configurations.

In Fig. 1(a)–(d), we can see the structural influence of the 5CB physisorption on G. Specifically, the presence of 5CB induces a flexion Δd of G perpendicular to the surface with the maximal distortion of 0.66 Å observed for the ECL structure. This distortion is of course dependent on the surface area Ω_{xy} of the calculation cell, and thus, relative comparisons of distortions are more meaningful than the magnitudes themselves. For instance, that the distortion measured at 0.25 Å for the INT structure is considerably smaller than for the ECL structure indicates the stress from the dispersion forces inducing the strain can vary appreciably between different binding structures. Therefore, we conclude there is an electromechanical coupling in the system that could be detected experimentally [47]. The flexion of G can be better understood from the planar averaged charge density difference shown in Fig. 2(a) or Fig. S1(a)–(d). Even though 5CB is mostly of aromatic and aliphatic composition, it induces rapid charge density fluctuations in the vicinity of the adsorption sites. These density fluctuations follow from electrostatics, which depends directly on the nonlocal dispersive forces in the presence of 5CB. While graphene has a large Young’s modulus, the flexural moduli of the monolayers, including graphene, are generally small, which allow even weak dispersive forces to be probed. The charge density fluctuations of the AC, INT, and ZZ structures [Fig. S1(b)–(d)], and concomitantly the flexions, however are quite similar. It therefore remains to be seen if the mesogen orientations could be measured indirectly through out-of-plane distortions.

While our Bader analysis showed that there is no ap-

preciable charge transfer between 5CB and G, the mesogen does induce a surface dipole for each orientation. The presence of the surface dipole could be inferred from the asymmetry in the charge density fluctuations. This dipole is likely the origin of the 5CB responsiveness reported in a recent experiment by Basu [23].

The Brillouin zones for the orthorhombic and hexagonal cells are shown in Fig. 3 for comparison of high symmetry points in the band structures of G and BN. We now turn to the electronic band structures for G [Fig. 4(a)]. The electronic band structure for 5CB on G in the INT structure is shown in Fig. 5(a) [Fig. S2(a)–(e)] [44] (see figures in Supplemental Material labeled with ‘S’ and figure number [44]). As expected, we have the band crossings at the Fermi level of the π bands at the corners of the hexagonal first Brillouin zone, see pristine G band structure in Fig. 4(a), which in Fig. 5(a) are located two thirds of the distance from Γ to X . The band dispersions at the crossings have the shape of Dirac cones. These cones are a characteristic of graphene, which follows from the symmetry between the two graphene sublattices. Because this crossing is not noticeably lifted in Fig. 5(a) [Fig. S2(a)–(e)], we conclude that the potential induced by the presence of 5CB does not appreciably discriminate between the sublattices. Thus, we can expect most of the electronic properties of graphene [48–50] to remain intact.

The states originating from 5CB are shown in red in Fig. S2(b)–(e). These states form bands that have relatively little dispersion, as is expected for localized adsorbates. Some electronic coupling however can be seen at band crossings near the high-symmetry points, in particular at the cell boundaries X and Y . The HOMO-LUMO states are found to straddle the Fermi level, which remains at the graphene Dirac point. This straddling is an example of a type-I alignment. Moreover, because the HOMO-LUMO states are approximately 1.5 eV from the Fermi level, the energy cost of moving electrons between 5CB and G effectively makes charge transfer negligible, which is consistent with our Bader analysis. The lack of charge transfer could be the reason that rapid response of the 5CB director field observed in experiment, in which graphene is used as an electrode [23, 51].

III.2. Boron nitride

Exchanging G for BN as the substrate, we obtain the structures in Fig. 1(e)–(h). As shown in Table I, the van-der-Waals distances between 5CB and BN are similar to that of the G case. This is expected as weak London dispersion forces again dominate the mesogen-substrate interactions. The binding energy is marginally weaker, ranging from -1.242 eV to -1.182 eV, a reduction of about 80 meV. This might be caused indirectly by the stronger in-plane polar bonding of BN [52, 53]. In any case, the dipole-dipole interactions between the mesogen and the surface are likely small compared to the London dispersion interactions. Again, the binding energy differ-

ences between our four structures are less than $k_B T$ and similar to those for 5CB/G, although with the strongest binding for the AC structure. Unlike in the G case, the biphenyl dihedral angle is not eclipsed, the angle ranging from -2.728° to -5.875° . The flexions for the AC, INT, and ZZ structures are on average 0.08 Å smaller than the corresponding flexions on G. The flexion for the ECL structure at $\Delta d = 0.22$ Å is three times smaller than for G, though as we shall see below, is a manifestation of the ECL flexion for 5CB/G being exceptionally large.

The charge fluctuations between 5CB/BN, shown in Fig. S1(e)–(h), display similar profiles to those of 5CB/G, although somewhat smaller in magnitude. Again, no charge transfer between the mesogen and the surface is observed in the band structure or the Bader analysis, which means that the fluctuations originate purely from dispersive forces.

As an insulator, BN has electronic ground state properties that are qualitatively different from G, see Fig. 4(a) and (b). For pristine BN, we find that the band structure in Fig. 4(b) contains a band gap of 4.4 eV, in line with past work [54–56]. The conduction and valence band edges again appear at the corners of the first Brillouin zone, indicated with green dashed lines noting the high symmetry point K , which in Fig. 5(b) is located two thirds of the distance from Γ to X . Unlike in the G case, the adsorption of 5CB leads to localized states inside the BN band gap, as can be seen in Fig. 5(b) [Fig. S3(b)–(e)]. Electrons could be excited into these states and be controlled optically, and thus BN could be a suitable substrate for optoelectronic applications [31, 57, 58].

The states in 5CB are not completely decoupled from BN. The HOMO interacts with the BN valence band, which is apparent in the highlighted part of the band structures in Fig. 5(d) [Fig. S3(b)–(e)]. Depending on the structure, the 5CB/BN interactions are able to shift the highest occupied state of the system between the Brillouin zone corners K and edges X . Such shifts, commonly observed in graphene nanoribbons [59–61], are caused by edge states that arise when a reflection symmetry is broken locally. These edge states are not present for potentials along the armchair direction, which is why no shift is observed in Fig. S3(c). Moreover, the effects of a broken reflection symmetry effectively cancels for most intermediate orientations, consistent with Fig. 5(d) [Fig. S3(d)]. For potentials along the zigzag directions however, the edge effect can be appreciable, which is indeed the case for the ECL and ZZ structures shown in Fig. S3(b) and S3(e). The edge states, which are in this case strongly coupled to the HOMO of 5CB, introduce band dispersion allowing the highest occupied state to shift along Γ – X , in this case to X .

The coupling of states between the mesogen and the substrate is not unique to the HOMO and the edge states. Such coupling can also be observed for the localized states in the gap. See the projected DOS in Fig. 6.

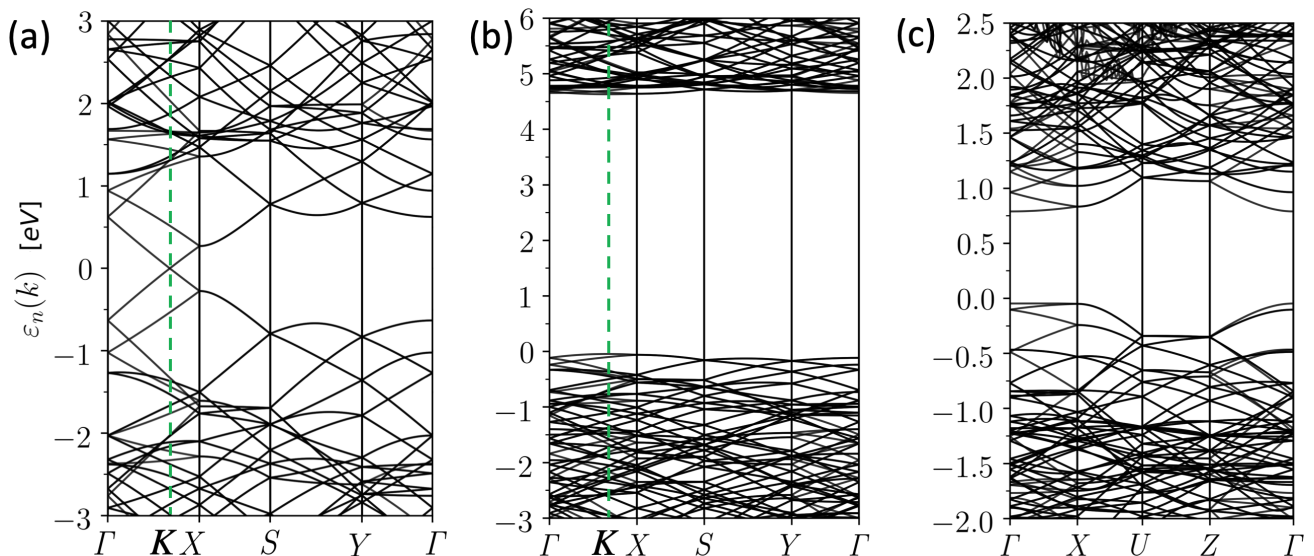


FIG. 4. Band structures for pristine nanosheets (a) G, (b) BN, and (c) BP. The Fermi level has been chosen to be zero.

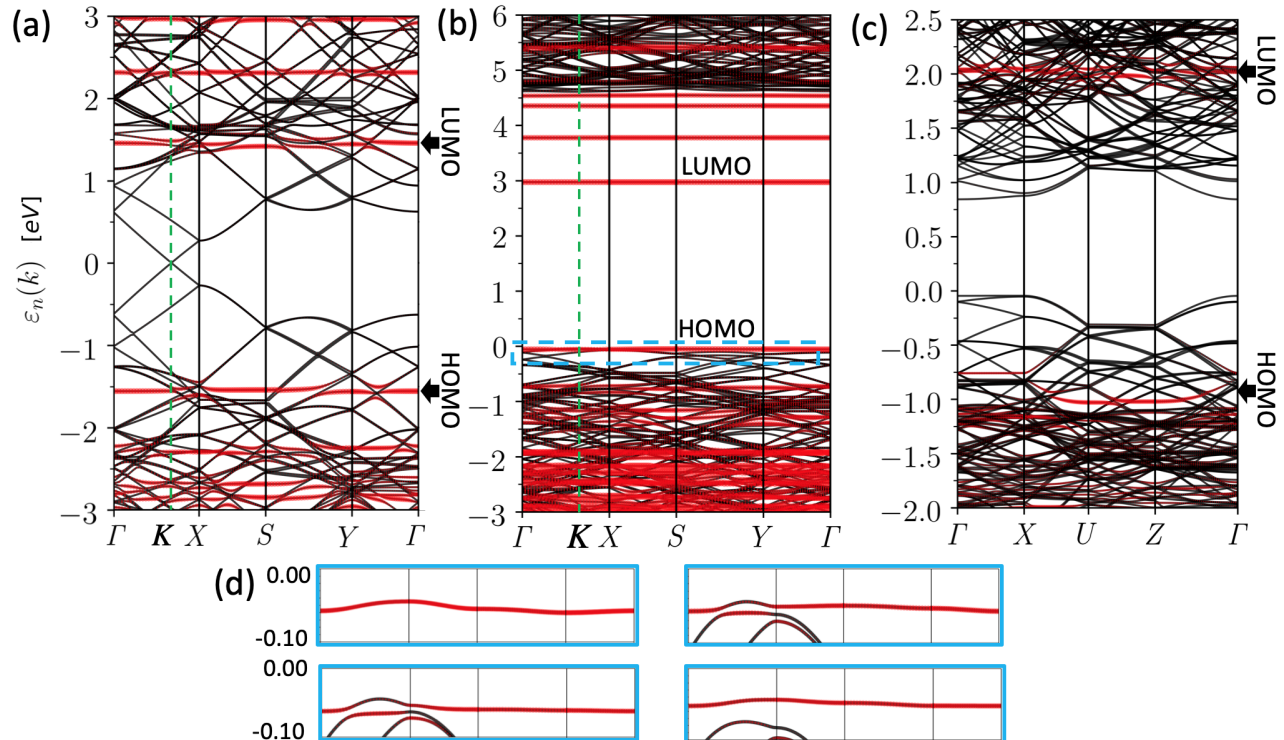


FIG. 5. Electronic structures for lowest energy systems (a) INT-5CB/G, (b) AC-5CB/BN and (c) INT-5CB/BP. (e) The insets below highlight the band dispersions in the interval $[-0.1, 0.0]$ eV for structures of BN in the ECL, AC, INT, and ZZ structures (left-to-right). The vertical green line marks the position of the high symmetry point K in the hexagonal Brillouin zone for G and BN, see Fig 3.

III.3. Phosphorene

Let us now exchange BN for BP as the substrate. The structures of 5CB/BP in Fig. 1(i)–(l) exhibit some notable differences with the previous substrates. First, we note that the flexion caused by 5CB on BP is relatively

small with Δd ranging from 0.07 \AA to 0.13 \AA . This is likely a result of BP having a planar truss structure, which is inherently more resistant to strain than the directly planar structure of G and BN [62–66]. Another qualitative difference is that the physisorption of 5CB on BP leads to much larger biphenyl dihedral angles, which as shown

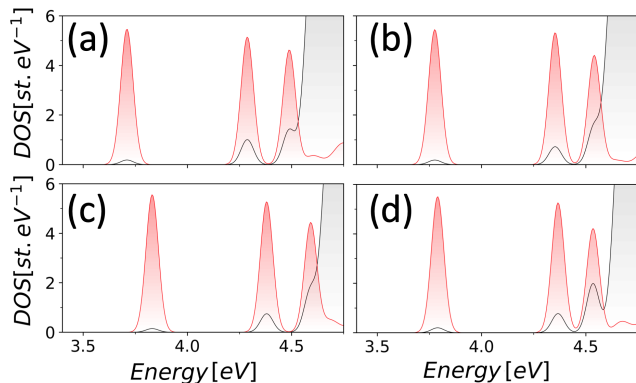


FIG. 6. The projected DOS of (a) ECL-5CB/BN (b) AC-5CB/BN, (c) INT-5CB/BN, and (d) ZZ-5CB/BN. The projections for 5CB are depicted in red.

in Table I ranges from -16.78° to -19.34° .

Despite the surface eclipsing being smaller, the binding for 5CB/BP is stronger than for both 5CB/G and 5CB/BN with the binding energy being on average approximately 21 meV lower for the four structures. This observation is also consistent with the slightly smaller mesogen-substrate distances for BP. The INT structure has the lowest binding energy at $E_B = -1.526$ eV, which makes this structure the lowest energy structure for BP as well as G, but not for BN. We also note that the binding energies for the ECL and ZZ structures are almost the same, which suggests that the ZZ structure on BP might not be metastable. In fact, it is quite possible that 5CB on BN will predominantly be found in an intermediate orientation, given that the INT structure has the lowest binding energy by 55 meV.

There are multiple possible explanations for why 5CB binds stronger to BP than to G or BN. One possible reason is that the out-of-plane puckering of the structure allows for apical, lone-pair $3p$ orbitals to penetrate deeper into the space between the mesogen and the substrate [64, 67]. The $3p$ orbitals have also been found to be responsible for its oxidative degradation in air [27, 68] and are thus generally expected to be more reactive than the rather inert orbitals in G and BN. Another explanation is that the charge redistribution caused by the adsorption of 5CB induces a much larger vertical dipole field in BP adding further to the London dispersion interactions. Note that this vertical dipole field can be observed in Fig. 2(c) [Fig. S1(i)-(l)], in which the planar-averaged charge density differences are larger in the vicinity of the phosphorene layer at 0 Å closest to the 5CB than in the layer at -2.3 Å and are dominated by one sign, in this case minus, indicating a net accumulation of electrons in this layer. The charge accumulation in the interval $[0, 2]$ Å is the largest in the INT structure, which is also consistent with the stronger binding for this particular

structure.

From the electronic band structure for pristine BP shown in Fig. 4(c), we find that the band gap is approximately 0.8 eV, and in good agreement with previous calculations [69]. As the HOMO-LUMO states of 5CB in Fig. 5(b) [Fig. S4(b)-(e)] straddle the conduction and valence band edges, we find that the band gap is fairly robust against the adsorption and orientation of 5CB. As the straddling is a type-I alignment, there is no direct charge transfer between 5CB and BP. However, charge density polarization is still present owing to the coupling of the 5CB and BP states, which leads to dispersion of the 5CB bands; see for instance the bands near -1 eV in Fig. S4(b)-(e). This coupling could potentially be used for tuning properties in applications, including optoelectronic and liquid crystal applications. Moreover, the substrate, possibly including a layer of 5CB, could potentially be used as an electrode material for such liquid crystal applications. Thus, BP could serve as an alignment layer and electrode for liquid crystal devices. Since BP is a semiconductor, the opportunity for engineering the core or tail of the 5CB or other members of the cyanobiphenyl family could open these systems to operate as an active component in an electro-optic device [6, 7, 70].

IV. CONCLUSION

In conclusion, we have explored the ground-state electronic properties of 5CB adsorbed onto G, BN, and BP. We have found that, despite dominant London dispersion and the absence of charge transfer, there are significant charge density fluctuations forming in the vicinity of the adsorbed mesogen. While each nanosheet displays strong binding to 5CB, 5CB/BP shows the strongest anchoring overall with the INT orientation being lowest in energy, which is likely caused by the puckering of the substrate. The energy alignment of the mesogen and substrate states was found to be type-I for all 2D substrates. Moreover, from the observed coupling between mesogen and substrate states, we conclude that chemical modification of 5CB could be used for tuning interface properties and concomitantly applications dependent on these properties. The interface properties could, for instance, act as the boundary conditions for the director field in a liquid crystal application. We expect such properties however, to be influenced by the presence of defects in the substrate, a topic for the future.

V. ACKNOWLEDGMENTS

This work has been supported by the Office of Naval Research, directly and through the **Naval Research Laboratory**. P.-A.-B. acknowledges the **ASEE Postdoctoral Fellowship Program** for support. There are no conflicts of interest to declare.

- [1] Q. Li, *Liquid Crystals Beyond Displays: Chemistry, Physics, and Applications* (Wiley, New York, 2012).
- [2] S. V. Shiyonovskii, O. D. Lavrentovich, T. Schneider, T. Ishikawa, I. I. Smalyukh, C. J. Woolverton, G. D. Niehaus, and K. J. Doane, *Mol. Cryst. Liq. Cryst.* **434**, 259/[587] (2005).
- [3] A. Czaplá, W. J. Bock, T. R. Woliński, P. Mikulic, E. Nowinowski-Kruszelnicki, and R. Dąbrowski, *Opt. Express* **24**, 5662 (2016).
- [4] V. G. Nazarenko, O. P. Boiko, M. I. Anisimov, A. K. Kadashchuk, Y. A. Nastishin, A. B. Golovin, and O. D. Lavrentovich, *Appl. Phys. Lett.* **97**, 263305 (2010).
- [5] T. Kato, M. Yoshio, T. Ichikawa, B. Soberats, H. Ohno, and M. Funahashi, *Nat. Rev. Mater.* **2**, 17001 (2017).
- [6] H. G. Gotjen, J. Kołacz, J. D. Myers, J. A. Frantz, R. Y. Bekele, J. Naciri, and C. M. Spillmann, *Proc. SPIE* **10526**, 105262B (2018).
- [7] J. A. Frantz, J. D. Myers, R. Y. Bekele, C. M. Spillmann, J. Naciri, J. Kołacz, H. G. Gotjen, V. Q. Nguyen, C. C. McClain, L. B. Shaw, and J. S. Sanghera, *J. Opt. Soc. Am. B* **35**, C29 (2018).
- [8] H. Milton, P. Brimicombe, P. Morgan, H. Gleeson, and J. Clamp, *Opt. Express* **20**, 11159 (2012).
- [9] R. L. Sutherland, V. P. Tondiglia, L. V. Natarajan, T. J. Bunning, and W. W. Adams, *Appl. Phys. Lett.* **64**, 1074 (1994).
- [10] C. Oh and M. J. Escuti, *Opt. Lett.* **33**, 2287 (2008).
- [11] X. Li, J. C. Armas-Pérez, J. P. Hernández-Ortiz, C. G. Argés, X. Liu, J. A. Martínez-González, L. E. Ocola, C. Bishop, H. Xie, J. J. de Pablo, and P. F. Nealey, *ACS Nano* **11**, 6492 (2017).
- [12] S. Savo, D. Shrekenhamer, and W. J. Padilla, *Adv. Opt. Mater.* **2**, 275 (2014).
- [13] H. Zhang, *ACS Nano* **9**, 9451 (2015).
- [14] G. R. Bhimanapati, Z. Lin, V. Meunier, Y. Jung, J. Cha, S. Das, D. Xiao, Y. Son, M. S. Strano, V. R. Cooper, L. Liang, S. G. Louie, E. Ringe, W. Zhou, S. S. Kim, R. R. Naik, B. G. Sumpter, H. Terrones, F. Xia, Y. Wang, J. Zhu, D. Akinwande, N. Alem, J. A. Schuller, R. E. Schaak, M. Terrones, and J. A. Robinson, *ACS Nano* **9**, 11509 (2015).
- [15] Y. Ren, Z. Qiao, and Q. Niu, *Rep. Prog. Phys.* **79**, 066501 (2016).
- [16] M. Boota, C. Chen, M. Bécuwe, L. Miao, and Y. Gogotsi, *Energy Environ. Sci.* **9**, 2586 (2016).
- [17] M. Zeng, Y. Xiao, J. Liu, K. Yang, and L. Fu, *Chem. Rev.* **118**, 6236 (2018).
- [18] X. Zhang, J. Grajal, J. Luis Vazquez-Roy, U. Radhakrishna, X. Wang, W. Chern, L. Zhou, Y. Lin, P.-C. Shen, X. Ji, X. Ling, A. Zubair, Y. Zhang, H. Wang, M. Dubey, J. Kong, M. Dresselhaus, and T. Palacios, *Nature* **566**, 368+ (2019).
- [19] P. Blake, P. D. Brimicombe, R. R. Nair, T. J. Booth, D. Jiang, F. Schedin, L. A. Ponomarenko, S. V. Morozov, H. F. Gleeson, E. W. Hill, A. K. Geim, and K. S. Novoselov, *Nano Lett.* **8**, 1704 (2008).
- [20] M. A. Shehzad, D. H. Tien, M. W. Iqbal, J. Eom, J. H. Park, C. Hwang, and Y. Seo, *Sci. Rep.* **5**, 13331 (2015).
- [21] R. Basu, D. Kinnamon, and A. Garvey, *J. Appl. Phys.* **118**, 114302 (2015).
- [22] A. Akbari, P. Sheath, S. T. Martin, D. B. Shinde, M. Shaibani, P. C. Banerjee, R. Tkacz, D. Bhat-tacharyya, and M. Majumder, *Nat. Commun.* **7**, 10891 (2016).
- [23] R. Basu and S. A. Shalov, *Phys. Rev. E* **96**, 012702 (2017).
- [24] R. Basu, *Phys. Rev. E* **96**, 012707 (2017).
- [25] R. Basu and A. Lee, *Appl. Phys. Lett.* **111**, 161905 (2017).
- [26] M. A. Shehzad, S. Hussain, J. Lee, J. Jung, N. Lee, G. Kim, and Y. Seo, *Nano Lett.* **17**, 1474 (2017).
- [27] B. A. Naqvi, M. A. Shehzad, J. Cha, K.-A. Min, M. F. Khan, S. Hussain, Y. Seo, S. Hong, J. Eom, and J. Jung, *Sci. Rep.* **8**, 12966 (2018).
- [28] M. A. Shehzad, J. Lee, S. H. Park, I. Akhtar, M. F. Khan, S. Hussain, J. Eom, J. Jung, G. Kim, C. Hwang, and Y. Seo, *2D Mater.* **5**, 045021 (2018).
- [29] P. Mei, Y. V. Kaneti, M. Pramanik, T. Takei, Ö. Dag, Y. Sugahara, and Y. Yamauchi, *Nano Energy* **52**, 336 (2018).
- [30] R. Basu and L. J. Atwood, *OSA Continuum* **2**, 83 (2019).
- [31] R. Basu and L. J. Atwood, *Opt. Mater. Express* **9**, 1441 (2019).
- [32] S. A. Fischer, J. Kołacz, C. M. Spillmann, and D. Gulycke, *Phys. Rev. E* **98**, 052702 (2018).
- [33] P. E. Blöchl, *Phys. Rev. B* **50**, 17953 (1994).
- [34] J. Hafner, *Comput. Phys. Commun.* **177**, 6 (2007).
- [35] J. Hafner, *J. Comput. Chem.* **29**, 2044 (2008).
- [36] G. Kresse and D. Joubert, *Phys. Rev. B* **59**, 1758 (1999).
- [37] J. P. Perdew, K. Burke, and M. Ernzerhof, *Phys. Rev. Lett.* **77**, 3865 (1996).
- [38] J. Paier, R. Hirschl, M. Marsman, and G. Kresse, *J. Chem. Phys.* **122**, 234102 (2005).
- [39] S. Grimme, J. Antony, S. Ehrlich, and H. Krieg, *J. Chem. Phys.* **132**, 154104 (2010).
- [40] S. Grimme, S. Ehrlich, and L. Goerigk, *Journal of Computational Chemistry* **32**, 1456 (2011).
- [41] P. E. Blöchl, O. Jepsen, and O. K. Andersen, *Phys. Rev. B* **49**, 16223 (1994).
- [42] E. Sanville, S. D. Kenny, R. Smith, and G. Henkelman, *J. of Comput. Chem.* **28**, 899 (2007).
- [43] W. Tang, E. Sanville, and G. Henkelman, *J. Phys.: Condens. Matter* **21**, 084204 (2009).
- [44] See Supplemental Material at [insert URL] for a complete data set of all structures and their band structures and charge density differences discussed in the main text.
- [45] S. Curtarolo, W. Setyawan, G. L. Hart, M. Jahnatek, R. V. Chepulskii, R. H. Taylor, S. Wang, J. Xue, K. Yang, O. Levy, M. J. Mehl, H. T. Stokes, D. O. Demchenko, and D. Morgan, *Comput. Mater. Sci.* **58**, 218 (2012).
- [46] J. Börk, F. Hanke, C.-A. Palma, P. Samori, M. Cecchini, and M. Persson, *J. Phys. Chem. Lett.* **1**, 3407 (2010).
- [47] J. Sun, M. Muruganathan, and H. Mizuta, *Sci. Adv.* **2**, e1501518 (2016).
- [48] A. K. Geim, *Science* **324**, 1530 (2009).
- [49] C. Xu, P. A. Brown, J. Lu, and K. L. Shuford, *J. Phys. Chem. C* **119**, 17271 (2015).
- [50] K. S. Novoselov, A. Mishchenko, A. Carvalho, and A. H. Castro Neto, *Science* **353**, aac9439 (2016).
- [51] S. A. Ivanov, A. Piryatinski, J. Nanda, S. Tretiak, K. R. Zavadil, W. O. Wallace, D. Werder, and V. I. Klimov, *JACS* **129**, 11708 (2007).
- [52] N. Marom, J. Bernstein, J. Garel, A. Tkatchenko, E. Joselevich, L. Kronik, and O. Hod, *Phys. Rev. Lett.*

- 105**, 046801 (2010).
- [53] A. Pakdel, Y. Bando, and D. Golberg, *Chem. Soc. Rev.* **43**, 934 (2014).
- [54] P. Miró, M. Audiffred, and T. Heine, *Chem. Soc. Rev.* **43**, 6537 (2014).
- [55] J. Wang, F. Ma, and M. Sun, *RSC Adv.* **7**, 16801 (2017).
- [56] C. E. Ekuma, V. Dobrosavljević, and D. Gunlycke, *Phys. Rev. Lett.* **118**, 106404 (2017).
- [57] Q. Tang, Z. Zhou, and Z. Chen, *J. Phys. Chem. C* **115**, 18531 (2011).
- [58] R. Zhang, B. Li, and J. Yang, *The Journal of Physical Chemistry C* **119**, 2871 (2015).
- [59] D. Klein, *Chemical Physics Letters* **217**, 261 (1994).
- [60] M. Fujita, K. Wakabayashi, K. Nakada, and K. Kusakabe, *Journal of the Physical Society of Japan* **65**, 1920 (1996).
- [61] D. Gunlycke, D. A. Areshkin, J. Li, J. W. Mintmire, and C. T. White, *Nano Letters* **7**, 3608 (2007).
- [62] C. Lee, X. Wei, J. W. Kysar, and J. Hone, *Science* **321**, 385 (2008).
- [63] N. Ding, C.-M. L. Wu, and H. Li, *Phys. Chem. Chem. Phys.* **16**, 23716 (2014).
- [64] L. Kou, C. Chen, and S. C. Smith, *J. Phys. Chem. Lett.* **6**, 2794 (2015).
- [65] Verma, Deepti and Hourahine, Ben and Frauenheim, Thomas and James, Richard D. and Dumitrică, Traian, *Phys. Rev. B* **94**, 121404 (2016).
- [66] A. Falin, Q. Cai, E. J. G. Santos, D. Scullion, D. Qian, R. Zhang, Z. Yang, S. Huang, K. Watanabe, T. Taniguchi, M. R. Barnett, Y. Chen, R. S. Ruoff, and L. H. Li, *Nat. Commun.* **8**, 15815 (2017).
- [67] A. Carvalho, M. Wang, X. Zhu, A. S. Rodin, H. Su, and A. H. Castro Neto, *Nat. Rev. Mater.* **1**, 16061 (2016).
- [68] A. J. Mannix, B. Kiraly, M. C. Hersam, and N. P. Guisinger, *Nat. Rev. Chem.* **1**, 0014 (2017).
- [69] H. Liu, A. T. Neal, Z. Zhu, Z. Luo, X. Xu, D. Tománek, and P. D. Ye, *ACS Nano* **8**, 4033 (2014).
- [70] C. K. Borah, P. K. Tyagi, S. Kumar, and K. Patel, *Comput. Mat. Sci.* **151**, 65 (2018).